Earthquakes and Structures, *Vol. 12, No. 1 (2017) 23-34*
DOI: https://doi.org/10.12989/eas.2017.12.1.023

Cyclic tests and numerical study of composite steel plate deep beam

Yi Hu[1a], Liqiang Jiang*[1,2] and Hong Zheng[1b]

[1]*School of Civil Engineering, Chang'an University, Xi'an 710061, China*
[2]*School of Civil Engineering, Southeast University, Nanjing 210018, China*

(Received June 28, 2016, Revised October 19, 2016, Accepted November 9, 2016)

Abstract. Composite steel plate deep beam (CDB) is proposed as a lateral resisting member, which is constructed by steel plate and reinforced concrete (RC) panel, and it is connected with building frame through high-strength bolts. To investigate the seismic performance of the CDB, tests of two 1/3 scaled specimens with different length-to-height ratio were carried out under cyclic loads. The failure modes, load-carrying capacity, hysteretic behavior, ductility and energy dissipation were obtained and analyzed. In addition, the nonlinear finite element (FE) models of the specimens were established and verified by the test results. Besides, parametric analyses were performed to study the effect of length-to-height ratio, height-to-thickness ratio, material type and arrangement of RC panel. The experimental and numerical results showed that: the CDBs lost their load-carrying capacity because of the large out-of plane deformation and yield of the tension field formed on the steel plate. By increasing the length-to-height ratio of steel plate, the load-carrying capacity, elastic stiffness, ductility and energy dissipation capacity of the specimens were significantly enhanced. The ultimate loading capacity increased with increasing the length-to-height ratio of steel plate and yield strength of steel plate; and such capacity increased with decreasing of height-to-thickness ratio of steel plate and gap. Finally, a unified formula is proposed to calculate their ultimate loading capacity, and fitting formula on such indexes are provided for designation of the CDB.

Keywords: composite steel plate deep beam; cyclic test; seismic performance; finite element method

1. Introduction

Infilled wall structural system is a research hotspot for its good performance to resist the lateral load produced by earthquake or wind. Generally, such infilled wall system is one of the most commonly used lateral loading resistance systems in building structures, especially in high-rise buildings. Because the traditional bare frame buildings have insufficient lateral stiffness and load-carrying capacity. Initial research focused on steel shear wall system (SSW) (Astaneh-Asl 2001), and the shear force of such wall system is carried by the tension field action of the steel plate after buckling occurred on it. The tension field will be transmitted directly to the frame columns, which may resulting in a great impact on the columns (Jahanpour *et al*. 2012). To prevent plastic hinges developing in the frame columns, strong columns must be designed to comply the design principle of "strong frame, weak wall" (Wang *et al*. 2015). In addition, to prevent the steel plate buckling too early, stiffening plate or composite steel plate have been proposed by some researchers (Astaneh-Asl 2001, Alavi and Nateghi 2013, Wang *et al*. 2015).

In the past decades, the reinforced concrete wall panel (RCWP) was introduced by Kahn and Hanson (1979) as a strengthening member to enhance the seismic performance of reinforced concrete (RC) frame. Such member separated the lateral load resisting member from frame column, and it was bolted to top and bottom beams. This research found that the bolted connection type of such member exhibited greater ductility and lower load-carrying capacity by comparing with the cast-in-place specimens. Such member was proposed as a retrofit/repair strategy for the RC frames (Horri *et al*. 1998), because the member could be precast constructed and connected with the frame through high-strength bolts. Engineered cementitious composite materials (ECC) were used to precast the RCWP for their good performance to dissipate energy generated from earthquake (Kesner and Bilington 2005), and series of experimental and theoretical investigations were performed by Kesner (2003). In recent years, many scholars have suggested that separating the infilled wall from the frame column, including steel frame with slit separated RC infill wall (Ju *et al*. 2012) and steel frame partially infilled with precast reinforced concrete wall (Jiang *et al*. 2016). In addition, there are many new types of wall panel system were proposed by the scholars. Jahanpour and Moharrami (2015) proposed the semi-supported type of steel shear wall, two semi-columns were constructed for the wall panel at two flanks to avoid non-economical design for the frame columns. Steel plate shear wall with tension-bracing system was introduced by kurata *et al*. (2012), four braces were constructed to support the steel wall panel. Other types of steel wall panel, such as double skin steel panels (Hong *et al*. 2011), steel plate shear wall connected to frame beams

*Corresponding author, Ph.D.
E-mail: jlq_1992@hotmail.com
[a]Ph.D. Student
E-mail: hyi_1991@163.com
[b]Professor
E-mail: cehzheng@chd.edu.cn

ISSN: 2092-7614 (Print), 2092-7622 (Online)

only (Guo *et al*. 2011) and self-centering steel plate shear wall with beam-only-connected web plate (Clayton *et al*. 2015) were proposed.

At researches presented here, composite steel plate deep beam (CDB) is proposed. CDB is precast constructed, and connected with frame beam with high-strength bolts. Such member consists of a steel plate deep beam with reinforced concrete panel attached to one side, and it has some advantages in comparison with other wall panels as following reasons. For it is clearly defined as a deep beam, the length of the CDB can be changed in a wide range, thus it can achieve a wide range of initial stiffness and loading capacity adjustment of frame structures. In addition, the main deformation of the deep beam is combining bending and shearing deformation, which is good for plastic developing of materials. Besides, the DB may exhibits better ductility for its bend-shearing deformation by comparing with the shear wall. Furthermore, the CDB can provide architectural space for installation of doors and windows for its flexible layout. The CDB can be easily assembled or removed for the bolted connection, thus it can be fastly and cost-efficiently fabricated in building repair or retrofit. Lastly, the RC panel can prevent the steel plate buckling too early, and provides temperature insulation as well as fire proofing to steel plate. nonlinear element models of CDBs were established and verified by test results. Finally, parametric analyses of CDBs In this study, tests of two composite steel plate deep beam with 1/3 scaled under cyclic loads were carried out. Besides, with different geometric dimension, material type and arrangement were performed, and a unified formula was proposed to calculate the ultimate loading capacity for designation of the CDB.

2. Test program

2.1 Details of specimens

Two 1/3 scaled composite steel plate deep beams (CDB) were tested in the experimental program. Fig. 1 and Fig. 2

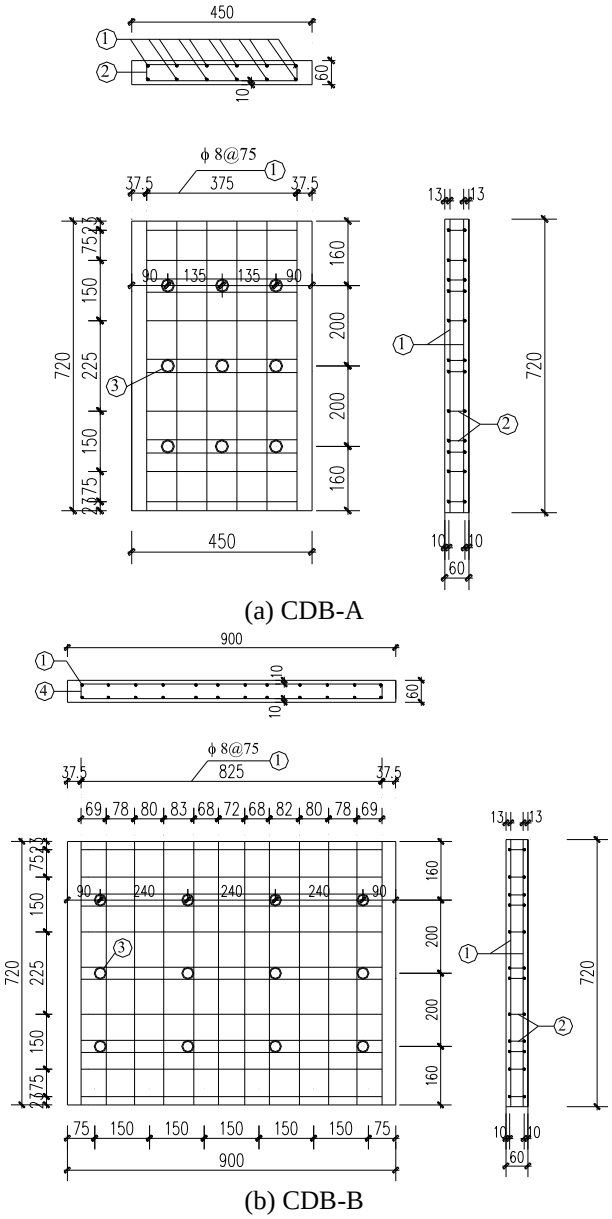

(a) CDB-A

(b) CDB-B

Fig. 1 Details of the RC panels for the CDBs

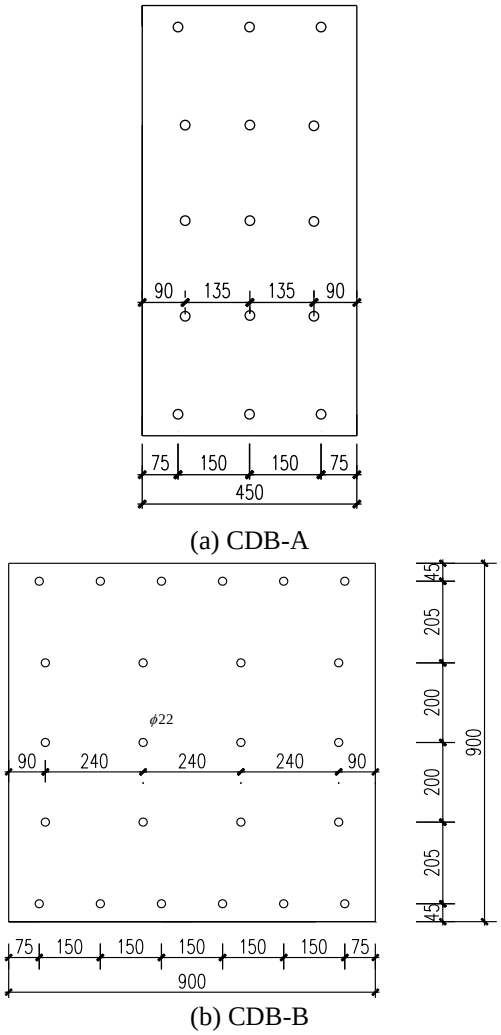

(a) CDB-A

(b) CDB-B

Fig. 2 Details of the steel plates for the CDBs

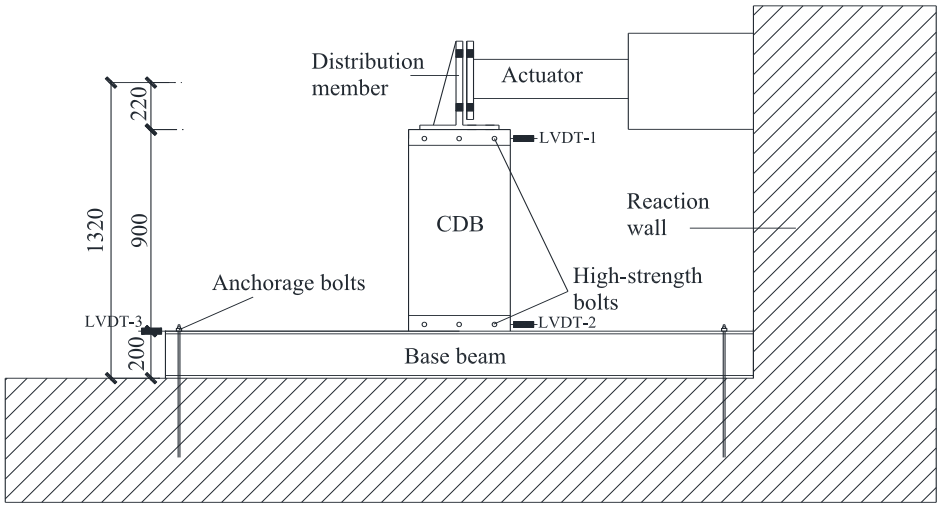

Fig. 3 Test setup

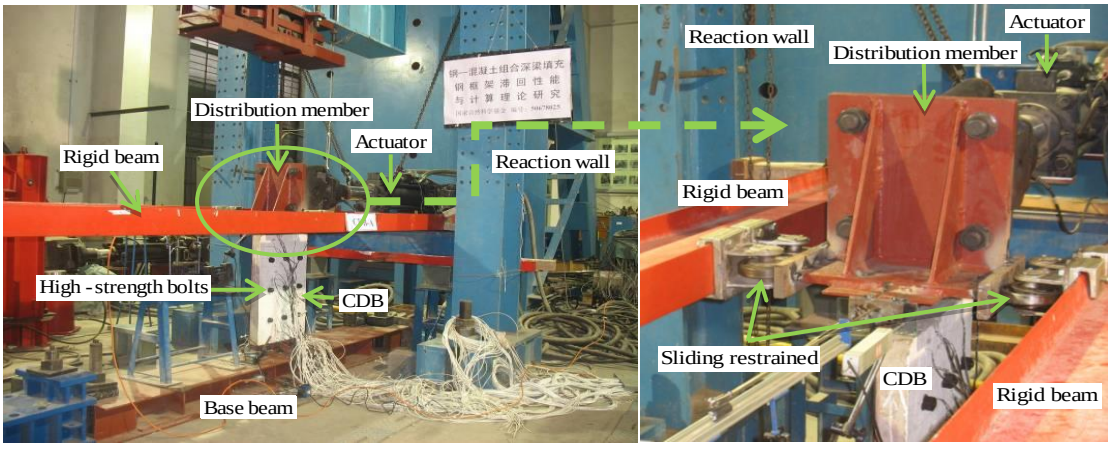

Fig. 4 Photographs of the test setup

show the detailed dimension of these specimens, and such specimens were constructed with different length-to-height ratio (CDB-A and CDB-B were 0.5 and 1.0, respectively). The height of the CDBs were 900 mm, and the length are 450 mm for CDB-A and 900 mm for CDB-B, respectively. To connect the steel plates and RC panels through high-strength bolts, 22 mm diameter bolt holes were driller on the steel plates and RC panels in advance, and the detailed dimension were presented in Fig. 1 and Fig. 2.

The vertical distance between two bolts centers was 810 mm, thus the effective height of the steel panel wall was 810 mm. The thickness of steel plates and RC panels were 4 mm and 60 mm, respectively. The reinforcing bars of the RC panel were arranged as a distance of 75 mm, and the diameter was 8 mm.

2.2 Test setup and instrumentation

Fig. 3 illustrates the setup of the test program. A distribution member was installed to ensure that the shear force can distribute to the CDBs more evenly, and such member was connected with the actuator through four M45 high-strength bolts. Each two angles at the both side of CDBs was installed back-to-back to clamp the CDBs, and M20 high-strength bolts were used to connected the angles and the CDBs. Such angles were connected with base beam and distribution member by M20 high-strength bolts, and the base beam was connected with the strong floor by anchorage bolts. Fig. 4 shows the photograph of the test setup. To avoid the out-of-plane deformation, two rigid beams were constructed to provide lateral support for the specimens. In addition, two pairs of sliding constraints were installed between the rigid beams and distribution member, as shown in Fig. 4. Fig. 5 shows the detailed connected status of the specimens and test device.

Two linear variable displacement transducers (LVDTs) were placed to record the lateral displacement of the specimen at the top and bottom sides, as shown in Fig. 3. In addition, a LVDT (LVDT 3) was placed at the base beam to measure the relative displacement between the base beam and strong floor. The mechanical behavior of the steel plate during the test was measured by rosette strain gauges, as shown in Fig. 6. Such gauges were placed on the steel plates so that the principal stresses at the interested locations could be acquired. There are also have numerous uniaxial strain gauges (as shown in Fig. 7) were placed along the steel bars to obtain the mechanical behavior of the

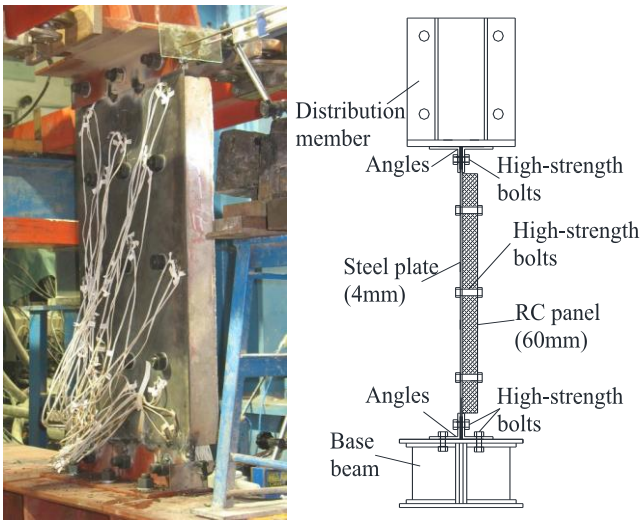

(a) (b)

Fig. 5 Connection details between the specimens and the test device

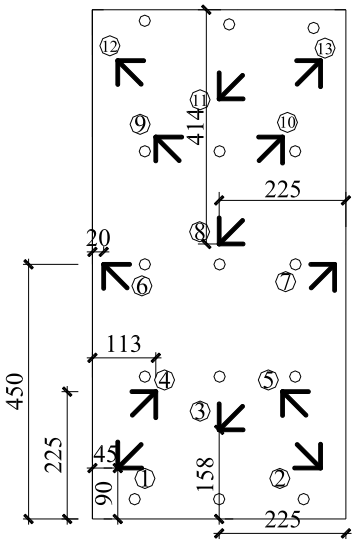

(a) CDB-A

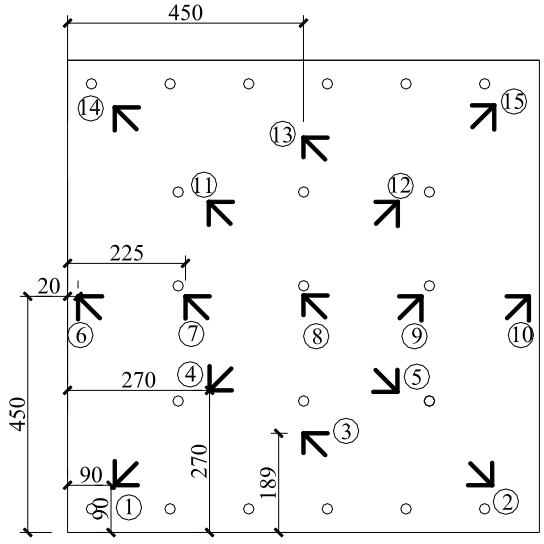

(b) CDB-B

Fig. 6 Arrangement of rosette strain gauges on the steel plate

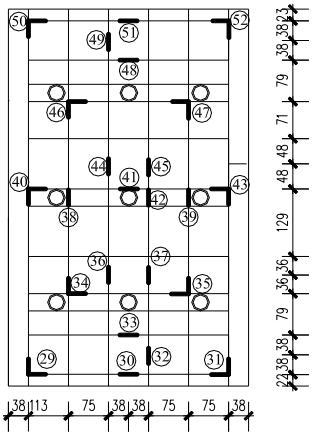

(a) CDB-A

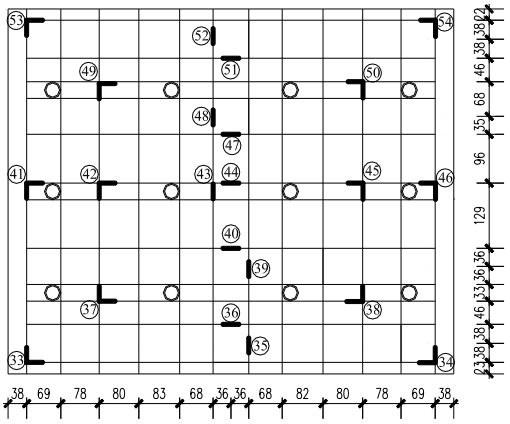

(b) CDB-B

Fig. 7 Arrangement of uniaxial strain gauges on the reinforcing bars

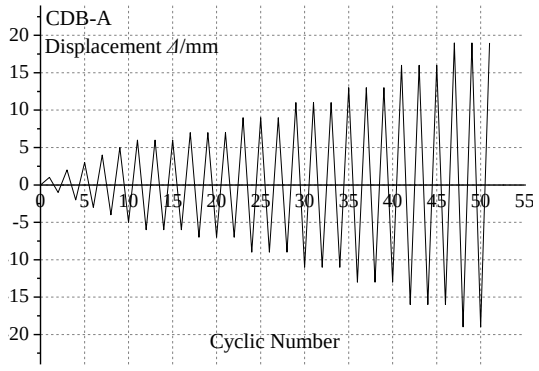

(a) CDB-A

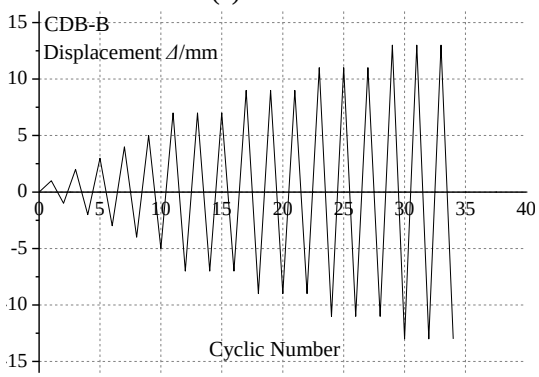

(b) CDB-B

Fig. 8 Loading patterns for the test specimens

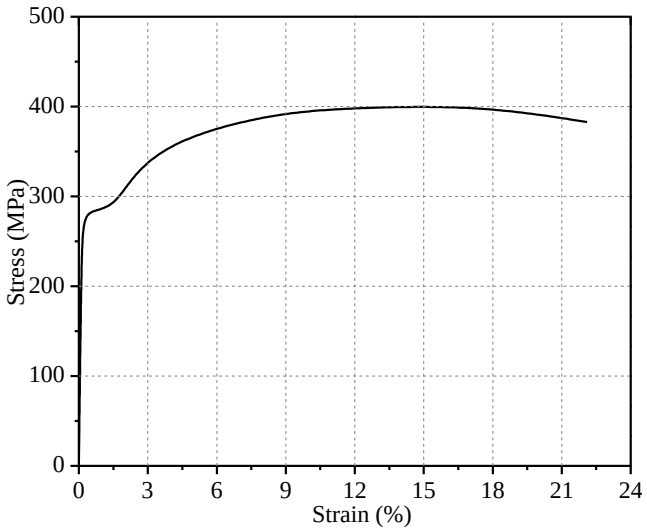

Fig. 9 Stress-strain relationship of steel

Table 1 Mechanical properties of reinforced concrete

Material	Property	Value
Concrete	Average cube compressive strength, f_{cu}	45.3 MPa
Reinforcing bar	Diameter, D	7.8 mm
	Yield stress, f_y	237.0 MPa
	Ultimate stress, f_u	536.7 MPa
	Elastic modulus, E_s	207.2×10^3 MPa
	Elongation ratio, δ	36.6%

RC plate. The target loading history for the specimens (as shown in Fig. 8) was set under displacement control according to the Chinese standard JGJ 101 (1996). At elastic stage, the lateral displacement was increased in multiples of 1 mm and repeated once time at each step. At elastic-plastic stage, that was repeated three times at each cycle. The yielding point was determine by two methods in the test programs: (1) a certain point of steel had been yield; (2) an obvious turning point was occurred in the *P-Δ* curve.

2.3 Material properties

To determine the mechanical properties of steel, three tensile coupons were cut from the tesed steel plate in accordance with the Chinese standard GB/T 228 (2002). The average value is presented in Fig. 9. The material of steel plates and angles were made of steel Q235B. The yield stress and yield ratio of the M20 pretension high-strength bolts were 800 N/mm^2 and 0.8, respectively. The pretension force applied to each bolt was 125 kN.

Table 1 shows the material properties of the concrete and the reinforcement bars. The concrete and reinforcement steel bars were designed as C30 and HPB235, respectively. Three groups of standard 28-day concrete cubes (150 mm×150 mm×150 mm) were taken from the batches of concrete and measured in accordance with the Chinese standard GB50081 (2002).

3. Test results and discussion

3.1 General observations and hysteretic behavior

The CDB-A exhibited in elastic stage when the lateral displacement was no more than 5mm, and the energy dissipation coefficient was less than 0.5. Crisp noise was produced from the high-strength bolts on the specimens at this loading step, and the steel plate started to deform due to the out-of-plane buckling occurred at the corners, as shown in Fig. 10(a). The principle strain on the steel plate at the bottom corner reached its yield value when the displacement reached 6mm, and the maximum out-of-plane deformation at the bottom corner was about 14mm. As the load increased, the out-of-plane buckling at the corners became more pronounced, and the relative deformation increased. The CDB-A reached its ultimate loading capacity when the displacement was 6.95mm, and the energy dissipation was about 0.8. After that, the force decreased sharply, and cracks appeared on the RC panel (shown in Fig. 10b) because of the local buckling was developing in the steel plate. As the displacement increased, the out-of-plane of the steel plate developed rapidly (shown in Fig. 10c), and the relative maximum out-of-plane deformation was about 48mm. Fig. 10(d) shows the failure mode of the CDB-A, and presents the residual deformation of steel plate.

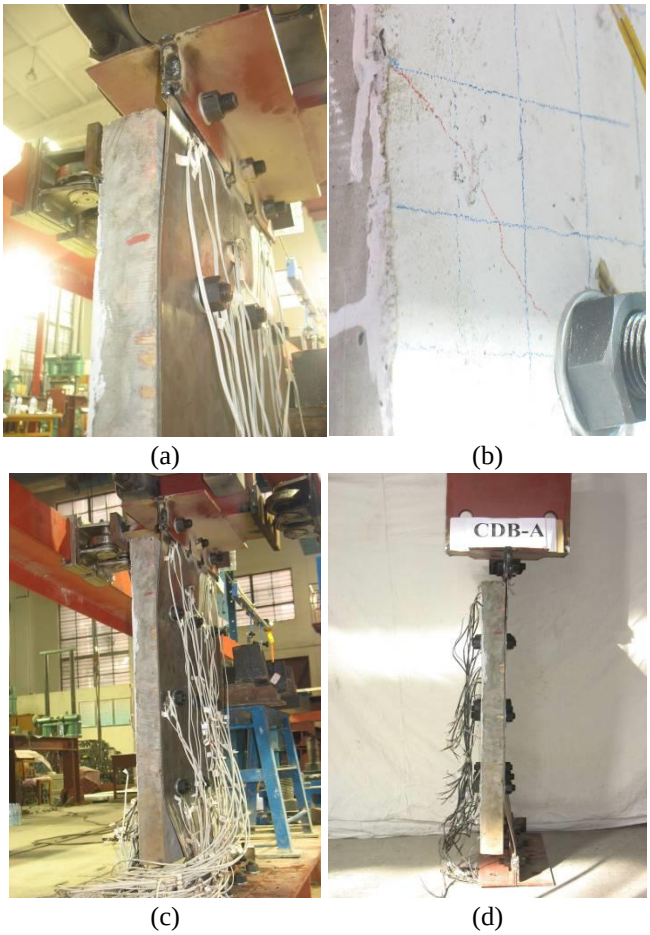

(a) (b)

(c) (d)

Fig. 10 Failure modes of the CDB-A

For the specimen CDB-B, it has a larger height-to-length ratio by comparing with the CDB-A. Out-of-plane buckling occurred at the bottom corner when the lateral displacement reached 5 mm, as shown in Fig. 11(a), and the out-of-plane deformation was about 6 mm at this loading level. The CDB-B reached its ultimately loading capacity when the displacement was 5 mm. After that, the load-carrying capacity of CDB-B slightly degraded. When the displacement reached 6 mm, local buckling occurred at the another bottom side, and crisp noise was produced from the high-strength bolts on the specimens at this loading step. The out-of-plane deformation of the buckled place was developing rapidly, and it was about 43 mm when the displacement reached 9 mm, as shown in Fig. 11(b). A micro crack formed at the bottom side of the steel plate at this loading level, and local buckling occurred at the top side of steel plate. When the displacement exceeded 9 mm, the force decreased sharply, and the out-of-plane deformation developed quickly. Fig. 11(c) shows the failure mode of the CDB-B, and the residual deformation of the CDB-B was presented in Fig. 11(d).

The hysteretic curves of the specimens are shown in Fig. 12, and the main results, such as lateral deformation, strength and ductility, are listed in Table 2. Where P_y and P_{max} are the yield load and maximum load of the tested specimen, respectively. Δ_y and Δ_{max} represent the yield and maximum displacement of the tested specimens, respectively. φ_y and φ_{max} are the yield and maximum drift of the specimens, respectively.

3.2 Ductility and energy dissipation

The ductility is represented by displacement ductility coefficient μ, which is one of the most important indexes to evaluate the seismic performance of the CDBs. Such coefficient can be calculated as the ratio of the failure displacement to the yield displacement, and the results of the test specimens are shown in Table 2. The failure displacement of a specimen is defined as the value when the lateral load declines to nearly 85% of the maximum lateral load (Jiang *et al*. 2014, Wang *et al*. 2015). The lateral displacement at yield point Δ_y was calculated by the equal-energy method, the definition of the method was showed in Fig. 13. The results show that the CDB-B exhibited better ductility than the CDB-A, indicating that the ductility of the specimens increase with the increasing of length-to-height ratio.

The energy dissipation coefficient E is proposed to describe the energy dissipation capacity of the specimens. Such value is another important index to evaluate the energy dissipation capacity of the specimens. The detailed

Table 2 Results of the tested specimens

Specimen	Yield			Maximum			Ductility
	P_y (kN)	Δ_y (mm)	φ_y (%)	P_{max} (kN)	Δ_{max} (mm)	φ_{max} (%)	$\mu=\Delta_{max}/\Delta_y$
CDB-A	24.30	5.2	0.64	26.45	7.8	0.96	1.50
CDB-B	71.97	3.9	0.48	76.79	9.1	1.12	2.33

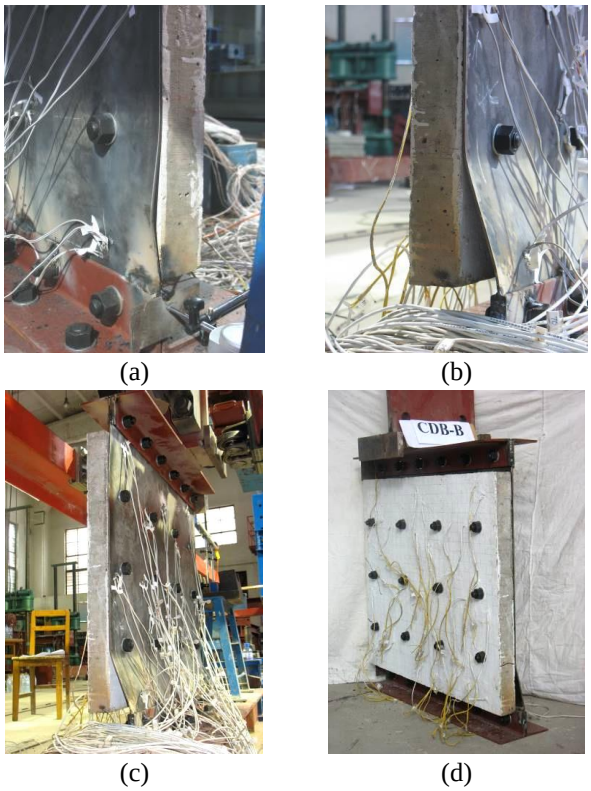

Fig. 11 Failure modes of the CDB-B

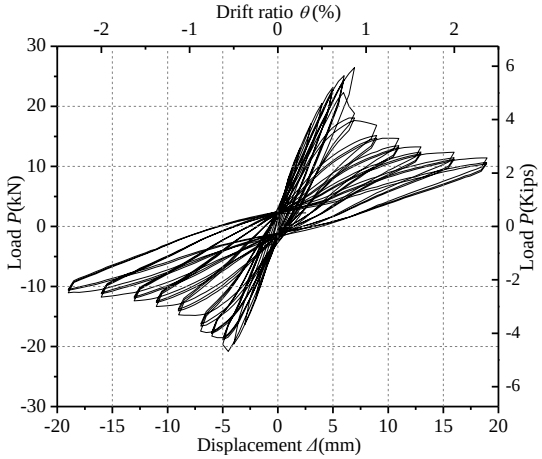

(a) CDB-A

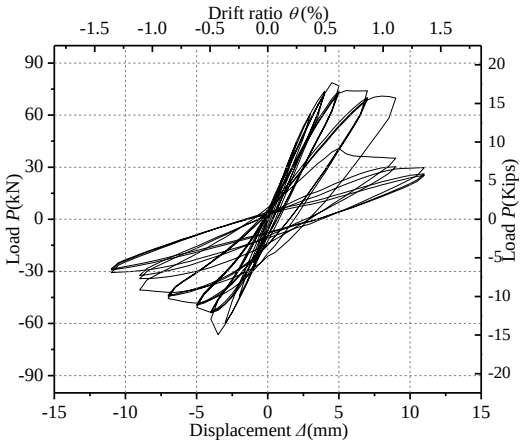

(b) CDB-B

Fig. 12 Hysteretic curves of the CDBs

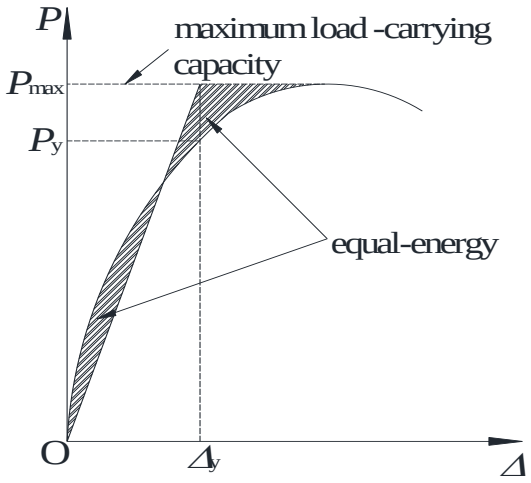

Fig. 13 Definition of the yield point for the specimens

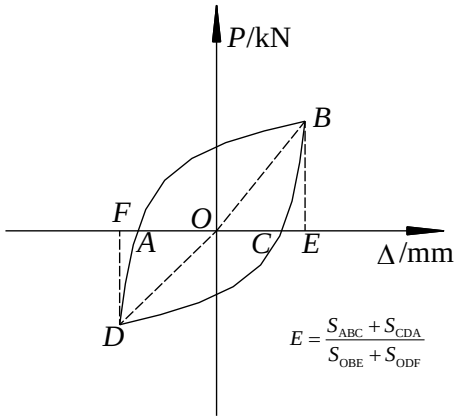

Fig. 14 Calculative method of energy dissipation coefficient

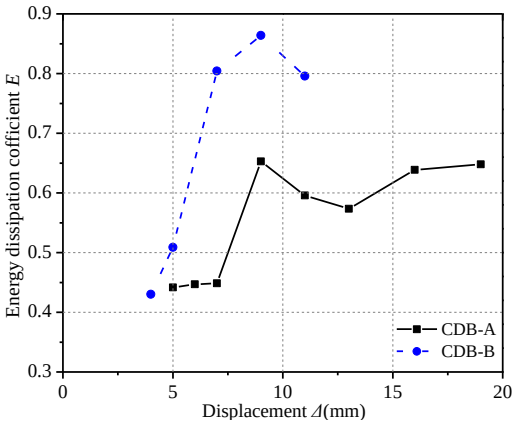

Fig. 15 Energy dissipation capacity curves

calculation was presented in Fig. 14 (Jiang *et al*. 2014, Wang *et al*. 2015), and Fig. 15 shows the energy dissipation coefficient of the test specimens. The results show that the energy dissipation coefficient increase with the increasing with the lateral displacement for the most part. The CDB-B exhibited better energy dissipation capacity than the CDB-A, indicating that the energy dissipation capacity of the specimens increase with the increasing of length-to-height ratio.

However, it should highlight that the effects of height-to-length ratio on ductility are not regular due to the limited number of specimens.

4. Numerical analysis

4.1 Finite element model and verification

To validate the finite model, the mechanical performance of the tested specimens was modeled by the ANSYS software and compared with the test results. In the numerical model, "Solid 65" and "REINF265" elements are chosen to simulate the mechanical behavior of concrete and reinforcements, respectively. Such 3D 8-node solid element is used for concrete to consider the cracks in tension and crippling in compression. "Shell 181" element is chosen to model steel plate, and such element has 4 nodes and 6 degrees of freedom per node. Same mesh sizes (30 mm) are performed for the steel plate and RC panel. Coupling method were used to simulate the behavior of high-strength bolts, the nodes of the connections were coupled with the same nodes on the steel plate and RC panel so that they have consistent deformations. The boundary conditions of the bottom and top side of steel plate are considered as fixed connection (at the bottom side, fixed the X, Y, Z, Rot X, Rot Y and Rot Z; at the top side, fixed the Y, Z, Rot X, Rot Y and Rot Z; the X-direction represents the direction that applying lateral loads) because friction type high-strength bolts were used at the boundary side. The lateral load is assumed as uniform load to apply at the top side of steel plate. In the finite element model (as shown in Fig. 16), such assumption is modeled by coupling the lateral displacement of the nodes at the top side of the steel plate, and such mechanical assumption was valid by Jiang *et al*. (2014, 2015).

As the steel plate and RC panel surfaces were contacted, so "CONTA170" and "TARGE174" elements are used to model the contacting behavior between RC panel and steel plate. The friction coefficient and contact pressure are specified as 0.2 and "hard", respectively. The initial defects are also considered in the modeling process. The lowest order buckling mode is performed as the imperfection shape of steel plate, and the maximum out-of-plane deformation is equal to 1/1000 of the length of the steel plate

$$\delta_{max} = L/1000 \tag{1}$$

where δ_{max} is the maximum out-of-plane deformation, and L is the length of the steel plate.

The constitutive equation of the steel plate is employing the material test results of the steel plate, as shown in Fig. 9. Besides, a bi-linear model is used for the reinforcements, and the material test results are used to model the elastic modulus, yield stress and ultimate stress of the reinforcements. Because the main function of RC panel is to restrain the out-of-plane deformation of steel panel wall, and no obvious damage observed on the RC panel. Therefore, the equation for concrete element is modeled as the equation of tension and compression for concrete, and the nominal tension and compression stress were specified as 4.5 MPa and 45.3 MPa, respectively. Such assumption

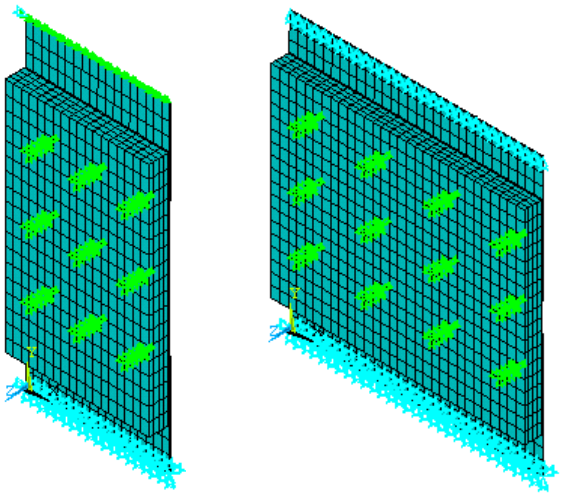

(a) CDB-A (b) CDB-B

Fig. 16 Finite element models

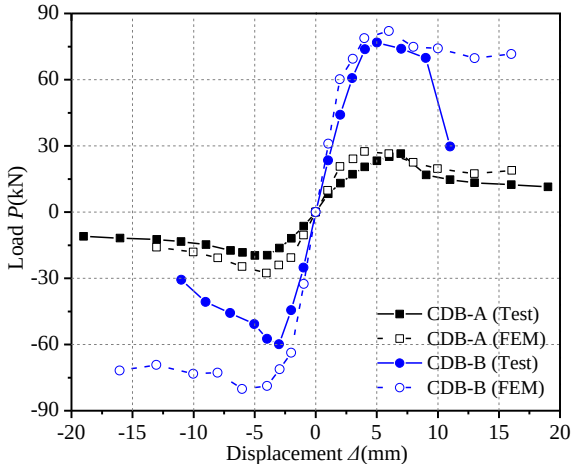

Fig. 17 Comparison of load-displacement curves between test and FEM results

Table 3 Comparison of the test and FEM results

Specimens		Δ_y (mm)	P_y (kN)	K_{ini} (kN/mm^2)	P_{max} (kN)	Δ_{max} (mm)
CDB-A	Test	5.2	24.30	8.30	26.45	7.8
	FEM	4.3	25.41	10.31	27.45	7.1
	Error	17.3%	4.6%	19.4%	3.9%	9.0%
CDB-B	Test	3.9	71.97	23.46	76.79	9.1
	FEM	3.1	77.12	33.08	82.00	13.05
	error	20.5%	7.2%	29.1%	6.8%	43.4%

can be valid by the following parametric analysis in the section 4.2.3.

Fig. 17 shows the calculated load-displacement curves of the tested specimens, and the detailed comparison between test and FEM results are presented in Table 3. It can be seen that there is a close agreement between the test results and FEM results in the elastic and elastic-plastic stage. For the CDB-A, the maximum shear force for test specimen and finite element model are 26.45 kN and 27.45 kN, respectively; for the CDB-B, the maximum shear force

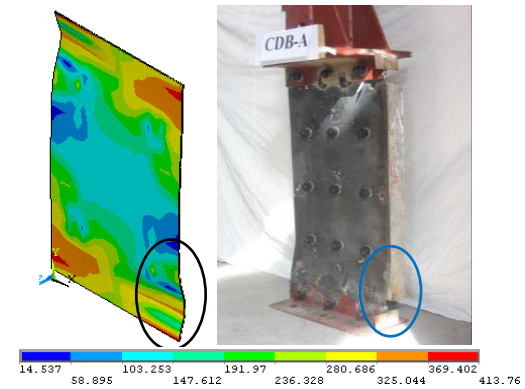

(a) CDB-A

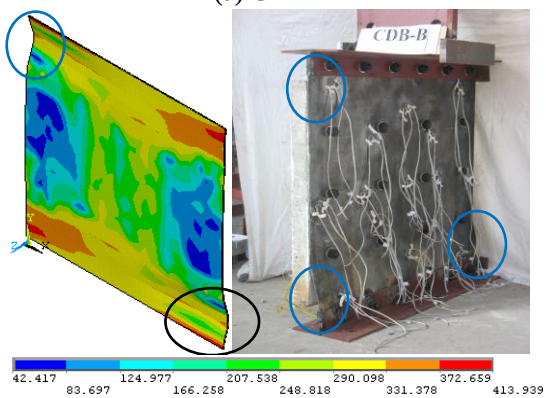

(b) CDB-B

Fig. 18 Comparison of failure mode between the test and FEM results

for the test specimen and model are 76.79 and 82.00, respectively. Though the elastic stiffness acquired from FE models are slight higher than the test results. This is because of the steel plate and RC panel were connected by high-strength bolts, relative shift may be occurred at the connections for the test, thus such coupling method used in these models may overestimate the real connected relationship between steel plate and RC panel. However, it can be seen that Fig. 18 shows that the failure modes obtained from FEM can predict the local buckling behavior and damage location of the test specimens. Besides, such results show that the differences between tests and FE models in maximum shear force value are no more than 7%. Thus it can be concluded that the numerical method can effective simulate the nonlinear behavior of the CDBs, which can be used for the following parametric study.

4.2 Parametric analysis of CDBs

To provide an analytical method that able to predict the responses of the CDBs depending on the geometrical and material information, a parametric analysis is performed based on the verified numerical simulation in Section 4.1. The following parameters are considered: length-to-height ratio of steel plate (α), height-to-thickness ratio of the gap (β_g), height-to-thickness of steel plate (β_s), material type and arrangement of RC panel.

In the parametric study, full-scaled CDBs are considered, and the height of steel plate is determined as

2700 mm. The thickness of steel plate is varied from 8 mm to 12 mm. The yield stress of steel plate includes three types: 235 N/mm^2 (Q235), 345 N/mm^2 (Q345) and 420 N/mm^2 (Q420); the compressive concrete stress includes three type: 25 N/mm^2 (C25), 30 N/mm^2 (C30) and 40 N/mm^2 (C40). Table 4 presents the detailed information of CDBs, and Fig. 19 shows the typical FEM models.

Therefore, formula on ultimate load capacity for the CDBs can be calculated by considering such parametric, and it can be given as

$$V_{\max} = f(\alpha, \beta_{gs}, \beta_s) f_y h t \tag{2}$$

where $f(\alpha, \beta_g, \beta_s)$ is a undetermined function associated with length-to-height ratio of steel plate (α), height-to-thickness ratio of the gap (β_g), height-to-thickness of steel plate (β_s); f_y is the yield strength of steel plate; h and t are the height and thickness of the steel plate, respectively.

4.2.1 Effect on geometric dimension of steel plate and RC panel

The length-to-height ratio of steel plate has great effect on the lateral loading capacity of CDB according to the test results. Six cases include from CDB 1-1 to CDB 1-6, the length of steel plate for these cases are varied from 1350 mm to 3000 mm. Fig. 20(a) shows the load-displacement curves of such cases, and the fitting curve and fitting formula are presented in Fig. 20(b).

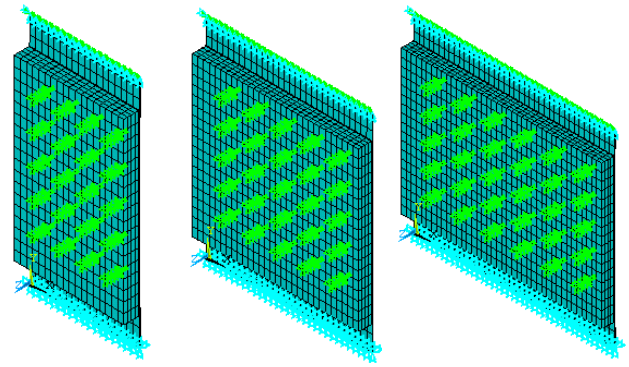

(a) CDB 1-7 (b) CDB 1-4 (c) CDB 1-6

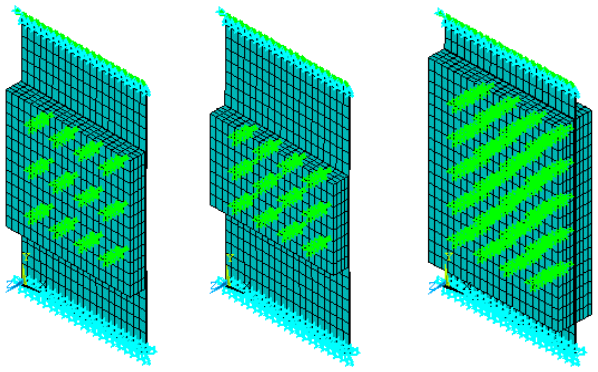

(d) CDB 1-9 (e) CDB 1-12 (f) CDB 4-1

Fig. 19 Part of FEM models for analyzed specimens

Table 4 Details of the CDBs for the parameter analysis (Unit: mm)

Specimens	Effects	l_s	t_s	l_c	h_c	Material type		Parameters		
						Steel	Concrete	α	β_{gs}	β_s
CDB 1-1	Length-to-height ratio of steel plate ($\alpha=l_s/h_s$)	1350	12	1350	2160	Q235	C30	0.5	29.2	225
CDB 1-2		1500	12	1500	2160	Q235	C30	0.556	29.2	225
CDB 1-3		1800	12	1800	2160	Q235	C30	0.667	29.2	225
CDB 1-4		2250	12	2250	2160	Q235	C30	0.833	29.2	225
CDB 1-5		2700	12	2700	2160	Q235	C30	1.0	29.2	225
CDB 1-6		3000	12	3000	2160	Q235	C30	1.111	29.2	225
CDB 1-7	Height-to-thickness ratio of the gap [$\beta_{gs}= (2700-h_c) / 2t_s$]	1500	12	1500	2160	Q235	C25	0.556	29.2	225
CDB 1-8		1500	12	1500	1920	Q235	C25	0.556	39.2	225
CDB 1-9		1500	12	1500	1680	Q235	C25	0.556	49.2	225
CDB 1-10		1500	12	1500	1440	Q235	C25	0.556	59.2	225
CDB 1-11		1500	12	1500	1200	Q235	C25	0.556	69.2	225
CDB 1-12		1500	12	1500	960	Q235	C25	0.556	79.2	225
CDB 2-1	Height-to-thickness ratio of steel plate ($\beta_s=h_s / t_s$)	1500	8	1500	2160	Q235	C25	0.556	29.2	337.5
CDB 2-2		1500	16	1500	2160	Q235	C25	0.556	29.2	168.75
CDB 2-3		1500	20	1500	2160	Q235	C25	0.556	29.2	135
CDB 3-1	Material type	1500	12	1500	2160	Q345	C25	0.556	29.2	225
CDB 3-2		1500	12	1500	2160	Q420	C25	0.556	29.2	225
CDB 3-3		1500	12	1500	2160	Q235	C40	0.556	29.2	225
CDB 4-1	Arrangement of RC panel	The steel plate was covered by RC panels on two sides, and other information is same with CDB 1-7.								

Note: l_s and t_s are the length and thickness of the steel plate, respectively; l_c and h_c are the length and height of RC panel, respectively

The results show a very high contribution of the length-to-height ratio up to a ultimate loading capacity. A higher length-to-height ratio of the CDB lead to higher loading capacity throughout all the different drift loading levels, and such results is also demonstrated by the tests. In addition, it can be concluded that an approximate linearity curve can be used to represent the relationship between the undetermined function f (Eq. (2)) and length-to-height ratio of steel plate, as shown in Fig. 20(b).

According to the test results presented in Section 3.1, it can be seen that local buckling occurred in the steel plate at the bottom and top sides, and then large out-of-plane deformation appeared at these positions. Such deformation decreased the effective area of the steel plate, which may result in lateral resistance degradation of the CDBs. Thus it is assumed that the height-to-thickness ratio of the gaps may also shows great impact on the maximum loading capacity of the CDBs. Six cases from CDB 1-7 to CDB 1-12, the height of RC panel for these cases are varied from 960 mm to 2160 mm, thus the height of the gaps are varied from 270 mm to 870 mm.

Fig. 21(a) shows the load-displacement curves of such cases. It can be concluded that the ultimate loading capacity of CDBs increases with decreasing of height-to-thickness ratio of the gap. The relationship between the the undetermined function f (Eq. (2)) and height-to-thickness ratio of the gap was fitted by an approximate linearity curve, as shown in Fig. 21(b).

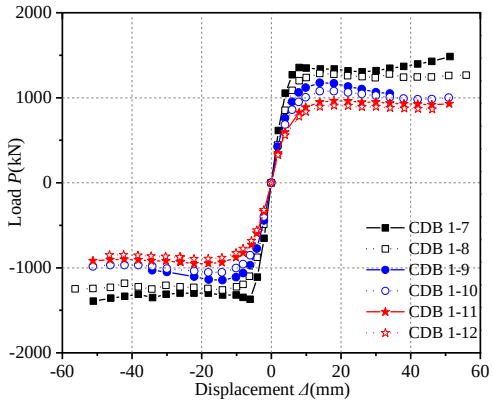

(a) Load-displacement relationship

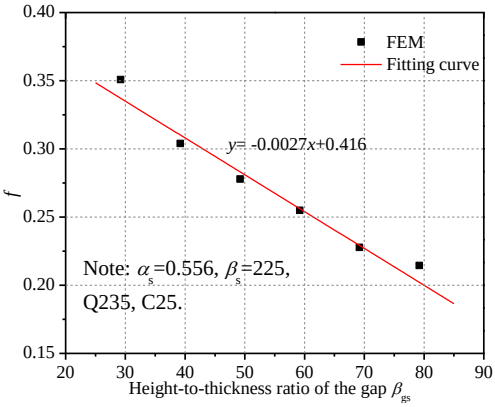

(b) Fitting curve

Fig. 21 Effect on height-to-thickness ratio of the gap

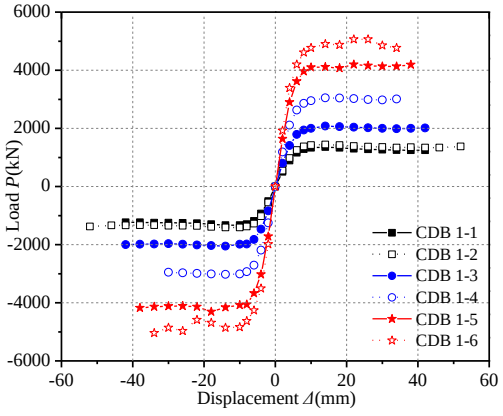

(a) Load-displacement relationship

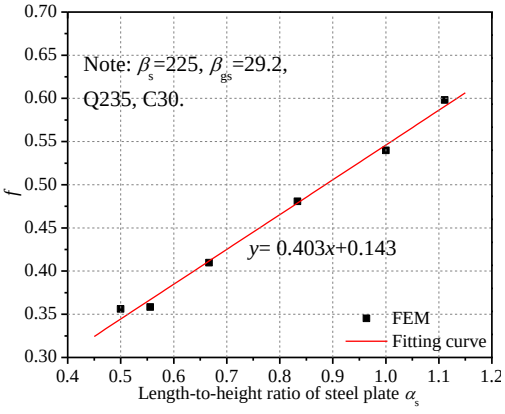

(b) Fitting curve

Fig. 20 Effect on length-to-height ratio α of steel plate

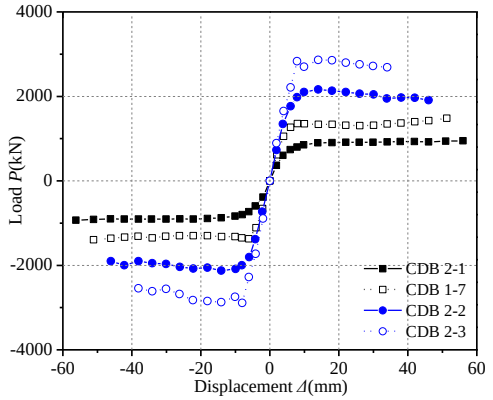

(a) Load-displacement relationship

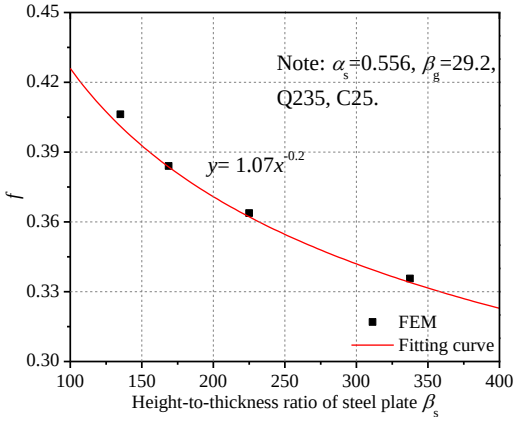

(b) Fitting curve

Fig. 22 Effect on height-to-thickness ratio of the steel plate

4.2.2 Effect on height-to-thickness ratio of steel plate

Height-to-thickness ratio of steel plate is another important index that effects the ultimate loading capacity of CDBs. In this study, four cases include CDB 1-7 and from CDB 2-1 to CDB2-3 are putted forward to analysis such index. The thickness of steel plate for these cases are varied from 8 mm to 20 mm, and the height-to- thickness ratio are varied from 135 to 337.5 relatively.

Fig. 22(a) shows the load-displacement curves of these cases, and it can be seen that the case with lowest height-to-thickness ratio exhibit the highest load-carrying capacity. Then a power function is used to fit the relationship between the undetermined function f (Eq. (2)) and height-to-thickness ratio.

4.2.3 Effect on material type and arrangement

Generally, the area of the generated tension field and the yield strength of the steel plate determine the load-carrying capacity of CDBs, thus the material type and arrangement of RC panel are also the main indexes for the ultimate loading capacity of CDBs. Each three cases is performed to analysis such effects. Q235, Q345 and Q420 grade steel are used to model the steel plate; C25, C30 and C40 grade concrete are conducted to model the RC panel. Fig. 23 shows the effects on yield strength of the steel plate, and Fig. 24 shows the effects on material type of RC panel. In addition, Fig. 25 presents the load-displacement curves of the CDB that covered by RC panel on two sides.

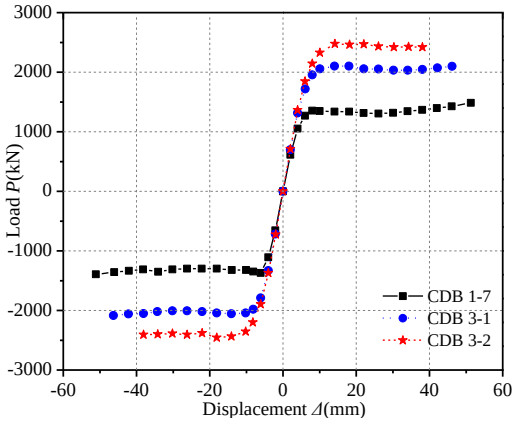

Fig. 23 Effect on yield strength of the steel plate

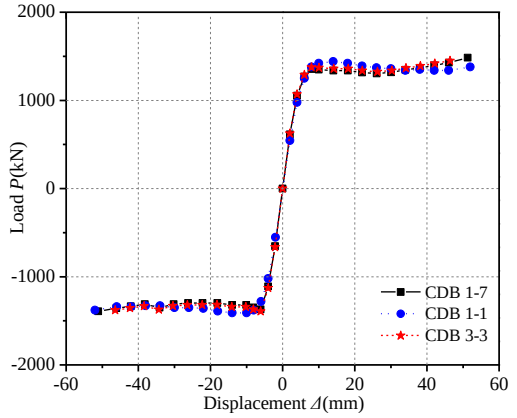

Fig. 24 Effect on material type of RC panel

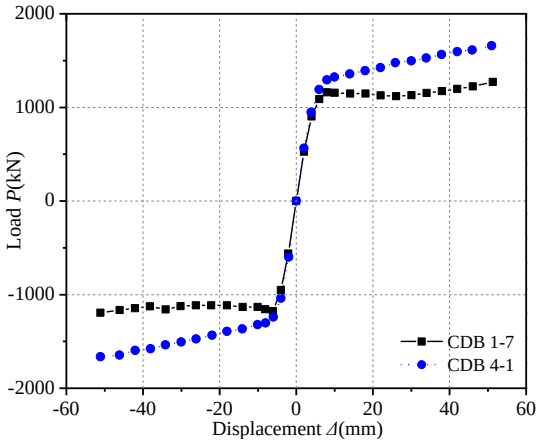

Fig. 25 Effect on arrangement of RC panel

According to the Fig. 23, the loading capacity of the CDBs increases with increasing of the yield strength of steel plate. The compressive strength of RC panel shows little impact on the loading capacity of CDBs according to the Fig. 24. Besides, the ultimate loading capacity of CDB covered with two sides panel increases about 30% than the same CDB covered with one side.

5. Conclusions

In this study, two 1/3-scaled composite steel plate deep beams were tested under cyclic loads to investigate their seismic performance. The nonlinear FE models of the CDBs were established and verified by the test results. Parametric analyses of CDB with different geometric dimension, material type and arrangement were carried out. The following conclusions can be dawn:

(1) The failure of the specimens started from local buckling of the steel plate; then the out-of-plane deformation developed rapidly and an inclined tension field formed to carry the lateral load; lastly, the CDBs lost their load-carrying capacity because of the large out-of plane deformation and yield of the tension field.

(2) Both load-carrying capacity and elastic stiffness of the specimens are significantly enhanced by increasing the length-to-height ratio of steel plate. In addition, the CDB with the higher length-to-height ratio exhibits better energy dissipation capacity and ductility.

(3) Nonlinear numerical method is used to model the CDB. The proposed finite model could effectively simulate the nonlinear behaviors of the CDB, including the failure modes and load-carrying capacity. Such FE method provides the tool for studying the performances of the CDBs.

(4) The indexes have great effect on lateral load-carrying capacity of the CDBs except for the strength of RC. The parametric analyses are carried out based on the proposed FE method. The ultimate loading capacity increases with increasing the length-to-height ratio of steel plate and yield strength of steel plate. Besides, such ultimate loading capacity increases with decreasing of height-to-thickness ratio of steel plate and gap.

(5) A unified formula is proposed to calculate the ultimate loading capacity of the CDBs, and fitting formula on such indexes are provided for the designation of the CDB.

Acknowledgments

This work was sponsored by the National Natural Science Foundation of China (50678025), the Science and Technology Activities Merit Aid for Foreign Experts of Shanxi Province (SLZ2008008). Which are gratefully acknowledged.

References

Alavi, E. and Nateghi, F. (2013), "Experimental study of diagonally stiffened steel plate shear walls", *J. Struct. Eng.*, **139**(11), 1795-1811.

Astaneh-Asl, A. (2001), *Seismic behavior and design of steel shear walls*, Steel TIPS rep., Structural Steel Educational Council, Moraga (CA).

Astaneh-Asl, A. (2002), *Seismic behavior and design of composite steel plate shear walls*, Steel TIPS rep., Structural Steel Educational Council, Moraga (CA).

Clayton, P.M., Berman, J.W. and Lowes, L.N. (2015), "Seismic performance of self-centering steel plate shear walls with beam-only-connected web plates". *J. Constr. Steel. Res.*, **106**(1), 198-208.

GB/T 228 (2002), *Tensile Test Method for Metal Materials at Room Temperature*, Chinese Standard Press, Beijing, China.

GB/T 50081 (2002), *Standard for Test Method of Mechanical Properties on Ordinary Concrete*, Chinese Architecture & Building Press, Beijing, China.

Guo, L.H., Rong, Q., Ma, X.B. and Zhang, S.M. (2011), "Behavior of steel plate shear wall connected to frame beams only", *Int. J. Steel. Struct.*, **11**(4), 467-479.

Horii, H., Kabele, P. and Takeuchi, S. (1998), "On the prediction method for the structural performance of repaired/ retrofitted structures", Fracture Mechanics in Concrete Structures: Proceedings of FRAMCOS-3, AEDIFICATIO Publishers, Freiburg, Germany.

Hong, S.G., Cho, B.H., Chung, K.S. and Moon, J.H. (2011), "Behavior of framed modular building system with double skin steel panels". *J. Constr. Steel. Res.*, **67**(2), 936-946.

Jahanpour, A., Jonsson, J. and Moharrami, H. (2012), "Seismic behavior of semi-supported steel shear walls", *J. Constr. Steel. Res.*, **74**(7), 118-133.

Jahanpour, A. and Moharrami, H. (2015), "Evaluation of behavior of the secondary columns in semi-supported steel shear walls", *Thin-Wall. Struct.*, **93**(3), 94-111.

JGJ 101 (1997), *Specification of Testing Methods for Earthquake Resistant Building*, Chinese Architecture & Building Press, Beijing, China.

Jiang, L.Q., Zheng, H., Yuan, X.S. and Sun, N. (2014), "The elastic mechanics calculation method for a steel plate deep-beam subjected to horizontal loads", *Eng. Mech.*, **31**(2), 146-163. (in Chinese)

Jiang, L.Q., Zheng, H., Liu, Y. and Yuan, X.S. (2014), "Experimental investigation of composite steel plate deep beam infill steel frame", *Int. J. Steel. Struct.*, **14**(3), 479-488.

Jiang, L.Q., Zheng, H., Zhao, P. and Wei, L. (2015), "Elastic buckling analysis on deep steel plate girders subjected to horizontal loading", *Pro. Steel Build. Struct.*, **17**(2), 1-6. (in Chinese)

Jiang, L.Q., Zheng, H. and Hu, Y. (2016), "Seismic behaviour of a steel frame partially infilled with precast reinforced concrete wall", *Adv. Struct. Eng*., **19**(10), 1637-1649.

Ju, R.S., Lee, H.J., Chen, C.C. and Tao, C.C. (2012), "Experimental study on separating reinforced concrete infill walls from steel moment frames", *J. Constr. Steel. Res.*, **71**(4), 119-128.

Kahn, L.F. and Hanson, R.D. (1979), "Infill walls for earthquake strengthening", *J. Struct. Div.*, **105**(ST4), 283-296.

Kesner, K.E. (2003), *Development of seismic strengthening and retrofit strategies for critical facilities using engineered cementitious composite materials*, Ithaca, NY: Cornell University.

Kesner, K.E. and Bilington, S.L. (2005), "Investigation of infill panels made from engineered cementitious composites for seismic strengthening and retrofit", *J. Struct. Eng.*, **131**(11), 1712-1720.

Kurata, M., Leon, R.T., DesRoches, R. and Nakashima, M. (2012), "Steel plate shear wall with tension-bracing for seismic rehabilitation of steel frames", *J. Constr. Steel. Res.*, **71**(4), 92-103.

Wang, M., Yang, W.G., Shi, Y.J. and Xu, J. (2015), "Seismic behaviors of steel plate shear wall structures with construction details and materials", *J. Constr. Steel. Res.*, **107**(4), 194-210.

Wang, M., Shi, Y.J., Xu, J., Yang, W.G. and Li, Y.X. (2015), "Experimental and numerical study of unstiffened steel plate shear wall structures", *J. Constr. Steel. Res.*, **112**(9), 373-386.

CC